ELSEVIER

Physica C 311 (1999) 197–210

PHYSICA C

ab-plane optical properties of Ni-doped $Bi_2Sr_2CaCu_2O_{8+\delta}$

H.L. Liu [a,*], D.B. Tanner [a], H. Berger [b], G. Margaritondo [b]

[a] *Department of Physics, University of Florida, Gainesville, FL 32611, USA*

[b] *Institute de Physique Appliquée, Ecole Polytechnique Fédérale de Lausanne, PHB Ecublens, 1015 Lausanne, Switzerland*

Received 14 July 1998; accepted 28 October 1998

Abstract

The *ab*-plane optical reflectance of single crystal of $Bi_2Sr_2Ca(Cu_{1-x}Ni_x)_2O_{8+\delta}$, for $x = 0.0215$, has been measured from 80 to 40 000 cm^{-1} (10 meV–5 eV) and at temperatures between 20 and 300 K. Through Ni substitution, the optical conductivity shows a broad peak at about 400 cm^{-1}, which grows in intensity and shifts to lower frequency as the temperature is reduced. We suggest that this peculiar low-frequency feature is associated with the significant disorder induced by Ni impurities. Analysis of the conductivity within the framework of the two-component and the one-component pictures indicates that the main effect of Ni substitution is to increase impurity scattering rate. There is no evidence of a rapid drop in the free carrier scattering rate near T_c. An estimate of the low-frequency spectral weight shows that Ni reduces the carrier density in the CuO_2 plane: each Ni removes one carrier. Below T_c, a sum-rule evaluation finds the superconducting condensate contains about a fifth of the total doping-induced, or two thirds of the free-carrier oscillator strength in the normal state. The strength of the condensate is horizontally offset from the Uemura line, with a smaller superfluid density than implied by T_c. This decreased superfluid density in the CuO_2 plane could be connected with the effect of impurity-induced disorder.

PACS: 74.25.Gz; 74.62.Dh; 74.72.Hs; 78.30.−j

Keywords: Infrared spectroscopy; Optical reflectivity; Superconductor

1. Introduction

The effect of impurity substitutional doping on high-T_c superconductors has received a great deal of attention in recent years [1]. Particular interest arises about the influence of $3d$ transition-metal ions substituted for the in-plane copper atoms Cu(2) because it is generally believed that the most important element of the superconducting cuprates is the two-dimensional CuO_2 plane. Among the many possibilities, Ni and Zn are the only dopants for which there is substantial evidence for substitution in the CuO_2 planes. The most prominent change of electronic properties brought on by Ni and Zn substitution is the strong suppression of T_c, with Zn suppressing T_c at a rate (10 K/at.%) about twice that of Ni [1]. A further issue is the effect on T_c reduction of magnetic (Ni) vs. nonmagnetic (Zn) dopants [1]. Magnetic impurities are known to suppress T_c due to Abrikosov–Gor'kov pair breaking, [2,3] whereas Anderson's theorem [4] states that nonmagnetic impuri-

* Corresponding author. Department of Physics, University of Illinois at Urbana-Champaign, Urbana, IL 61801, USA. Tel.: +1-217-333-9019; Fax: +1-217-244-2278; E-mail: liu@uimrl7.mrl.uiuc.edu

0921-4534/99/$ - see front matter
PII: S0921-4534(98)00637-6

ties do not affect T_c. The effect of dopants on the superconducting properties of high-T_c materials is considerably different from conventional superconductors [1].

So far, a large number of experimental studies of Ni and Zn doping have concentrated on $YBa_2Cu_3O_{7-\delta}$ (Y123) systems. However, substitutional effects in Y123 can easily be confused by accompanying changes in oxygen content. In contrast, $Bi_2Sr_2CaCu_2O_{8+\delta}$ (Bi-2212) offers a simpler possibility to probe the intrinsic response of the CuO_2 planes in the presence of transition-metal dopants because there are no chains in these Bi-based compounds, although there is a superlattice structure along the *b*-axis.

In this paper, we discussed the *ab*-plane reflectance of a $Bi_2Sr_2Ca(Cu_{1-x}Ni_x)_2O_{8+\delta}$ ($x = 0.0215$) single crystal over the frequency range from far-infrared to the near-ultraviolet in both normal and superconducting states. To the best of our knowledge, there have been no reports on the far-infrared optical properties of Ni-doped Bi-2212 samples. We will compare our Ni-doped data with results for undoped Bi-2212 samples [5–8] in an effort to learn how Ni substitution affects the *ab*-plane optical properties at temperatures above and below T_c.

2. Experimental techniques and data analysis

Our single crystal of $Bi_2Sr_2Ca(Cu_{1-x}Ni_x)_2O_{8+\delta}$ ($x = 0.0215$) was grown using the conventional self-flux method. The Ni content was determined by electron-probe microanalysis (EPMA). The crystal had a dimension about $4 \times 4 \times 0.1$ mm^3. The sample shows an onset of T_c in AC susceptibility at 70 K, with transition width $\Delta T_c = 5$ K. Characterizations of DC resistivity and angle-resolved ultraviolet photoemission spectroscopy (ARUPS) have also been performed on similar samples [9]. The resistivity data shows a linear temperature variation and a large residual resistivity [9].

The *ab*-plane optical reflectance has been measured from 80–40 000 cm^{-1} (10 meV–5 eV). We used a Bruker IFS 113v Fourier transform spectrometer to cover the frequency range from 80 to 4000 cm^{-1} and a flow cryostat for the temperature variation from 300 K down to 20 K. Room-temperature reflectance spectra were collected from 1000 up to 40 000 cm^{-1} by using a Perkin-Elmer 16U grating spectrometer. Under a microscope, the sample had optically flat and shiny surface, so no attempt was made to coat the surface with aluminum to correct for scattering loss.

The optical conductivity was derived by the Kramers–Kronig analysis of the reflectance spectrum. To perform this transformation, one needs to extrapolate the reflectance at both low and high frequencies. In the normal state, we modeled the reflectance using the Drude–Lorentz model, while below T_c the two-fluid model was used. Then, we used the fitted results to extend the reflectance from the lowest frequency measured in the experiment to $\omega \approx 0$. The Hagen–Rubens relation was also used as an extrapolation to low frequencies above T_c. Above 100 cm^{-1} the optical conductivity is not sensitive to the choice of low-frequency approximation. For high frequency extrapolation, the temperature dependent data up to 4000 cm^{-1} was joined smoothly with the measured high frequency room temperature result. Between 40 000 and 320 000 cm^{-1}, the reflectance was merged with the pure Bi-2212 results of Terasaki et al. [10]; beyond this frequency range a free-electron-like behavior of ω^{-4} was assumed.

We will evaluate on optical conductivity using a partial sum rule, estimating the spectral weight in terms of the effective number of carriers per CuO_2 plane [11];

$$\left[\frac{m}{m^*}\right] N_{\mathrm{eff}}(\omega) = \frac{2mV_{\mathrm{cell}}}{\pi e^2 N_{\mathrm{Cu}}} \int_0^{\omega} \sigma_1(\omega')\,\mathrm{d}\omega', \qquad (1)$$

where m^* is the effective mass of the carriers, m is the free-electron mass, V_{cell} is the unit cell volume, and N_{Cu} is the number of CuO layers per unit cell. Here, we use $N_{\mathrm{Cu}} = 2$ for the Bi-2212 materials. The effective mass is taken as the free-electron value. $N_{\mathrm{eff}}(\omega)$ is proportional to the number of carriers participating in the optical excitations up to $\hbar\omega$.

3. Comparison of Ni-doped to pure $Bi_2Sr_2CaCu_2O_{8+\delta}$

The upper panel of Fig. 1 compares the reflectance at 300 K to pure Bi-2212 sample over the

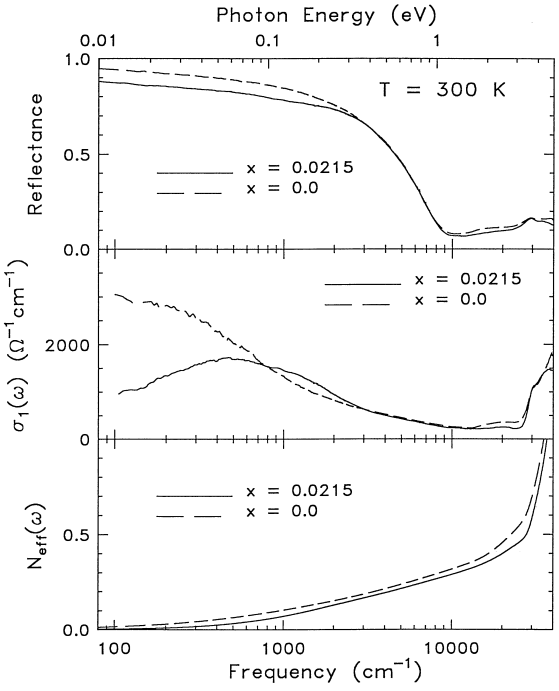

Fig. 1. The 300 K reflectance (upper), real part of conductivity (middle), and the effective carrier numbers (lower) spectra of the pure (dashed line) and Ni-doped (solid line) $Bi_2Sr_2CaCu_2O_{8+\delta}$ crystals in the entire frequency range [6–8].

entire measured frequency range. The most striking difference is that the reflectance of Ni-doped crystal is significantly lower below 3000 cm^{-1} than in the pure material, indicating that Ni impurities modify the electronic structure near the Fermi level. In contrast, the reflectance above 3000 cm^{-1} up to a plasma minimum around 10 000 cm^{-1} is not affected by Ni substitution. At higher frequencies, two interband transitions are evident. The strength of the 16 000 cm^{-1} (2 eV) peak for the Ni-doped sample is weaker than that for the undoped case, while the intensity of 30 000 cm^{-1} (3.8 eV) band is similar for both samples. All of the above observations for the Ni-doped crystal are quite different from those in the carrier-depleted case [8], where the rearrangement of spectral weight occurs from 0 eV up to several electron volts.

A comparison of the room-temperature optical conductivity for the pure and Ni-doped Bi-2212 crystals is presented up to 40 000 cm^{-1} in the middle panel of Fig. 1. In pure system, the low-frequency conductivity is dominated by free-carrier behavior (a Drude absorption at $\omega = 0$). Ni modifies significantly the $\sigma_1(\omega)$ spectra. The Drude peak centered at $\omega = 0$ in the pure crystal changes into a peak positioned at about 400 cm^{-1} in the Ni-doped sample. Ni substitution decreases the far-infrared conductivity but increases the mid-infrared conductivity in the 1000 to 3000 cm^{-1} range. As the frequency increases above 10 000 cm^{-1}, we observe a decrease in the strength of the first interband transition at $\sim$16 000 cm^{-1} in the Ni-doped samples. At the same time, the band shifts to higher frequencies. There is general agreement that the broad band near 16 000 cm^{-1} is characterized by O 2p and Cu 3d charge-transfer (CT) excitation. Thus, it is reasonable to speculate the observed discrepancy in the CT band between the pure and Ni-doped crystals reflects different electron configuration: $d_{x^2-y^2}$ hole for Cu^{2+} and $d_{x^2-y^2}d_{3z^2-r^2}$ holes for Ni^{2+}. Support for this speculation comes from comparing the CT peak of insulators La_2CuO_4 with that of La_2NiO_4. In La_2CuO_4, the CT excitation is seen at about 2 eV, while in La_2NiO_4 the CT gap moves towards 4–5 eV [12]. With regard to the second electronic peak near 30 000 cm^{-1}, both samples roughly resemble each other. The excitation is possibly associated with transitions occurring in the Bi–O layers and not in the CuO_2 planes. Still, the identification of this band remains controversial [8,13–15].

In the lower panel of Fig. 1, we plot the room-temperature $N_{\rm eff}(\omega)$ results of the pure and Ni-doped crystals. In both materials, $N_{\rm eff}(\omega)$ at first increases rapidly in the infrared region, begins to level off near 8000 cm^{-1}, and then rises again above the onset of the CT band. However, the overall magnitude for the Ni-doped crystal is slightly smaller than of the pure sample in the studied spectral range. In order to give a quantitative value of the effective number of carriers, we take as the number of $N_{\rm eff}(\omega)$ at $\sim$14 500 cm^{-1}, just before the influence of the CT band begins to dominate the results. Then, the spectral weight below the onset of the CT gap corresponds to an effective number of total carriers per copper, $N_{\rm tot}$, of $\sim$0.38 and 0.34 for the pure and Ni-doped samples, respectively. Our results provide evidence that Ni likely substitutes as Ni^{2+} for Cu^{2+n}. The 0.03–0.04 reduction in $N_{\rm tot}$ for our Ni-doped sample with a Ni content of $c_{\rm Ni} = 4.3$ at.% suggests that each Ni removes one carrier.

4. Temperature dependence of Ni-doped $Bi_2Sr_2CaCu_2O_{8+\delta}$

4.1. Reflectance spectrum

The *ab*-plane reflectance of the Ni-doped crystal is shown between 80 and 2000 cm^{-1} at temperatures above and below T_c in Fig. 2. The absolute value of the room-temperature reflectance is over 70% for $\omega < 2000$ cm^{-1}. When the sample is cooled, there is a substantial temperature dependence in the reflectance. The reflectance increases rapidly with decreasing temperature. Below 75 K, it is also interesting that above 600 cm^{-1} there is no temperature dependence. In the superconducting state, the reflectance is not close to unity down to the low frequency limit of our measurements. Such behavior is different from that of undoped Bi-2212, for which the reflectance is quite high, and is greater than 99% below ~ 200 cm^{-1} at $T \ll T_c$ [6–8]. This difference clearly suggests that Ni impurities disturb the superconductivity. Another feature worth noting is the shoulder-like structure developing in the reflectance at $\omega \sim 500$ cm^{-1}, a common behavior in many of the cuprate superconductors [16].

4.2. Conductivity and dielectric function

The real part of optical conductivity $\sigma_1(\omega)$ is shown below 2000 cm^{-1} and for several temperatures in Fig. 3. There is unusual behavior of optical conductivity below 2000 cm^{-1}. The 300 K spectrum consists of a broad maximum approximately 400 cm^{-1}, which grows in intensity and shifts to lower frequency as the temperature is lowered. Below T_c, we observe a decrease of low-frequency spectral weight associated with the formation of the superconducting condensate. However, a strong peak near 100 cm^{-1} is still visible down to 20 K. This peculiar feature is present through the whole measured temperature range. The inset of Fig. 3 compares the 20 K data for Ni-doped to undoped Bi-2212 [6–8]. There is clearly a much larger conductivity with former case. Here, we must emphasize that the conductivity maximum peak itself is not an experimental artifact. We checked the low-frequency extrapolation does not affect the result qualitatively. Furthermore, the DC conductivity values at 300 and 100 K, reported by Quitmann et al. [9] for crystals similar to ours, are marked along the vertical axis of Fig. 3. They are much lower than the value of the frequency

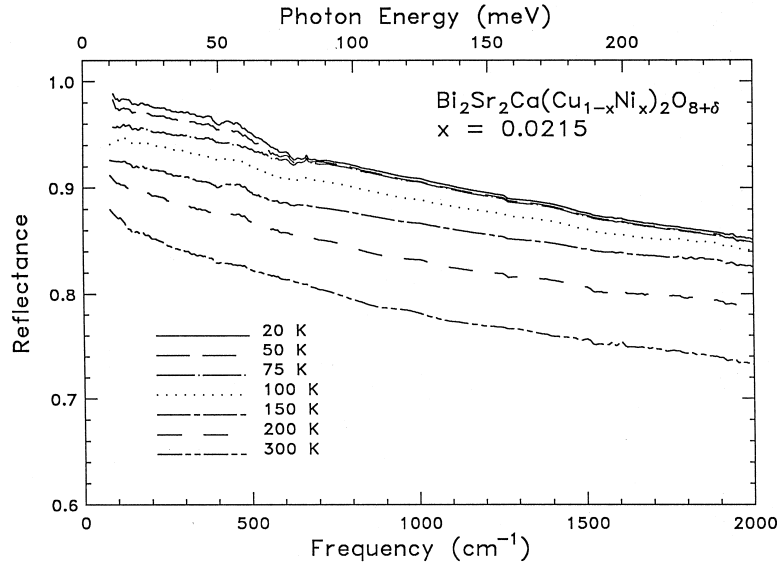

Fig. 2. The *ab*-plane optical reflectance of Ni-doped $Bi_2Sr_2CaCu_2O_{8+\delta}$ from 80 to 2000 cm^{-1} and at temperatures above and below T_c.

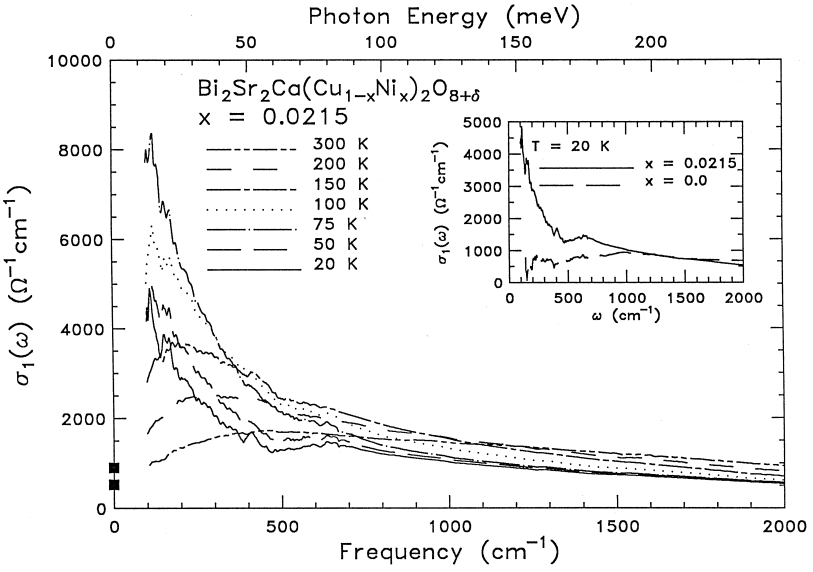

Fig. 3. The real part of the optical conductivity for Ni-doped $Bi_2Sr_2CaCu_2O_{8+\delta}$, calculated by Kramers–Kronig analysis of the reflectance spectra. The symbols on the vertical axis show the DC conductivities at 75 and 300 K for crystals similar to ours [9]. The inset displays the 20 K $\sigma_1(\omega)$ spectra of the pure (dashed line) and Ni-doped (solid line) Bi-2212 crystals [6–8].

dependent conductivity maximum, but there is a fair agreement between the far-infrared $\sigma_1(\omega \to 0)$ and the DC conductivities. A similar broad low frequency peak has been observed for other high-T_c superconducting materials, which are either intrinsically or deliberately disordered including $Bi_2Sr_2CuO_6$ (Bi-2201) [17], $Pb_2Sr_2(Y/Ca)Cu_3O_8$ [18], and $Tl_2Ba_2CuO_{6+\delta}$ (Tl2201) [19]. The conductivity peak was also seen in the response of Y123 single crystal after low energy He^+ ion irradiation [20] and Zn-doped or Ni-doped Y123 films [21] as well as *a*-axis Zn-doped $YBa_2Cu_4O_8$ (Y124) [22]. Considering all of the above, we believe that the observed finite frequency peak is an intrinsic response of the disordered CuO_2 plane.

The Kramers–Kronig-derived real part of the frequency-dependent dielectric function, $\epsilon_1(\omega)$, is shown in Fig. 4. At high frequencies, $\epsilon_1(\omega)$ is negative at all temperatures and the zero crossing corresponds to the location of the screened plasma frequency. Below 500 cm^{-1} the dielectric function rises dramatically to positive values for the normal-state curves, but drops sharply upon entry into the superconducting state. We attribute the positive low-frequency $\epsilon_1(\omega)$ at high temperatures to the gradual development of the strong peak in far-infrared $\sigma_1(\omega)$. When $T < T_c$, in a system where most of the normal-state carriers collapse into the superconducting δ function, then the real part of the dielectric function becomes $\epsilon_1(\omega) = \epsilon_\infty - \omega_{pS}^2/\omega^2$, where ϵ_∞ is background dielectric associated with the high frequency interband transitions and ω_{pS} is the plasma frequency of the condensate. As a result, the superconducting condensate is sufficiently strong to give the large negative value of $\epsilon_1(\omega)$ in the low-frequency region at 50 and 20 K.

4.3. Two-component model

In order to gain insight into the unusual aspect of the optical conductivity, we describe the normal-state optical properties in term of a phenomenological two-component model. The complex dielectric function is written as

$$\epsilon(\omega) = \epsilon_1(\omega) + \frac{4\pi i}{\omega}\sigma_1(\omega) = \epsilon_\infty - \frac{\omega_{pD}^2}{\omega^2 + i\omega/\tau_D} + \sum_{j=1}^{N} \frac{\omega_{pj}^2}{\omega_j^2 - \omega^2 - i\omega\gamma_j}, \quad (2)$$

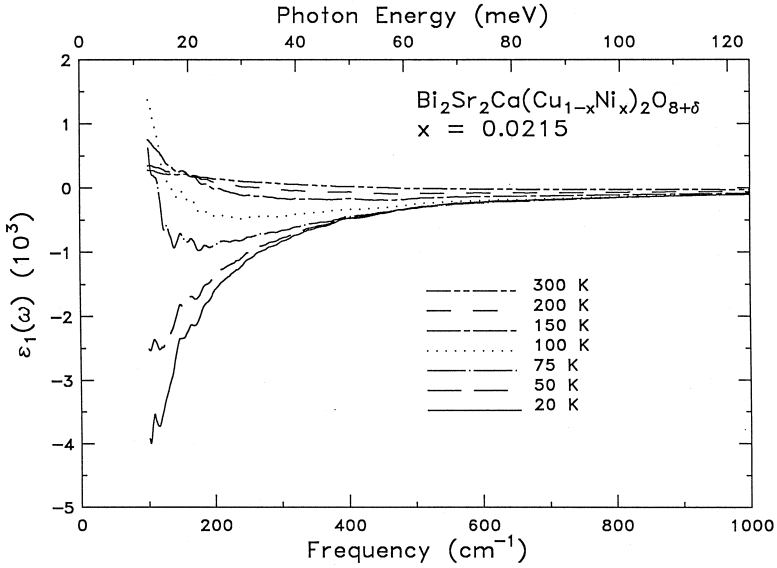

Fig. 4. The real part of the dielectric function $\epsilon_1(\omega)$ (from Kramers–Kronig transformation) at several temperatures for Ni-doped $Bi_2Sr_2CaCu_2O_{8+\delta}$.

where ϵ_∞ is a constant term, and ω_{pD} and $1/\tau_D$ are the plasma frequency and scattering rate of the Drude (free carrier) component, and ω_{pj}, ω_j, and γ_j are the oscillator strength, the resonant frequency, and the width of the jth Lorentz (bound carrier excitation) contribution. The real part of the optical conductivity is calculated from the imaginary part of the dielectric function $\sigma_1(\omega) = \omega\epsilon_2(\omega)/4\pi$.

The details of the fit are rather complicated because of the many parameters. We have tried to fit the room-temperature conductivity spectrum in the whole frequency range with a Drude part, four Lorentzian oscillators below 8000 cm^{-1} (not counting phonon), and three above the CT gap. We used the preliminary parameters and made a least-squares fit to the experimentally measured reflectance. Because the temperature-dependent data extend only to 4000 cm^{-1}, we fixed the parameters for the higher frequency oscillators with $\omega > 6000$ cm^{-1}. In addition, we fixed $\epsilon_\infty = 3.0$. Then we varied the Drude parameter and three mid-infrared oscillators to fit the measured reflectance below 4000 cm^{-1} at 200, 150, 100, and 75 K. The parameters are listed in Table 1. The results for the fit are compared to the low-energy portion ($\omega < 2000$ cm^{-1}) of the conductivity in Fig. 5.

In our fits, two absorption peaks appear in the mid-infrared region. One is around 1000 cm^{-1}, with its position shifting to a slightly lower frequency and its magnitude decreasing as the temperature is reduced. The other, at about 1875 cm^{-1}, has a small systematic temperature variation. In contrast, the lowest frequency Lorentz mode, which is near 400 cm^{-1} at 300 K, acquires a progressively more spec-

Table 1
Parameters of a two-component oscillator fit to the measured reflectance below 4000 cm^{-1} at 300, 200, 150, 100, and 75 K

	T				
	300 K	200 K	150 K	100 K	75 K
ω_{pD}	8280	8666	8687	8530	8657
$1/\tau_D$	1151	871	710	568	504
ω_{p1}	4124	5643	6842	7400	7768
ω_1	402	288	225	149	106
γ_1	821	559	413	276	182
ω_{p2}	9877	8926	7891	6906	5719
ω_2	1017	1014	966	955	950
γ_2	2623	2234	1839	1815	1774
ω_{p3}	8219	7749	8243	9391	10420
ω_3	1875	1866	1883	1857	1883
γ_3	7746	10711	12516	10529	8623

All units are in cm^{-1}.

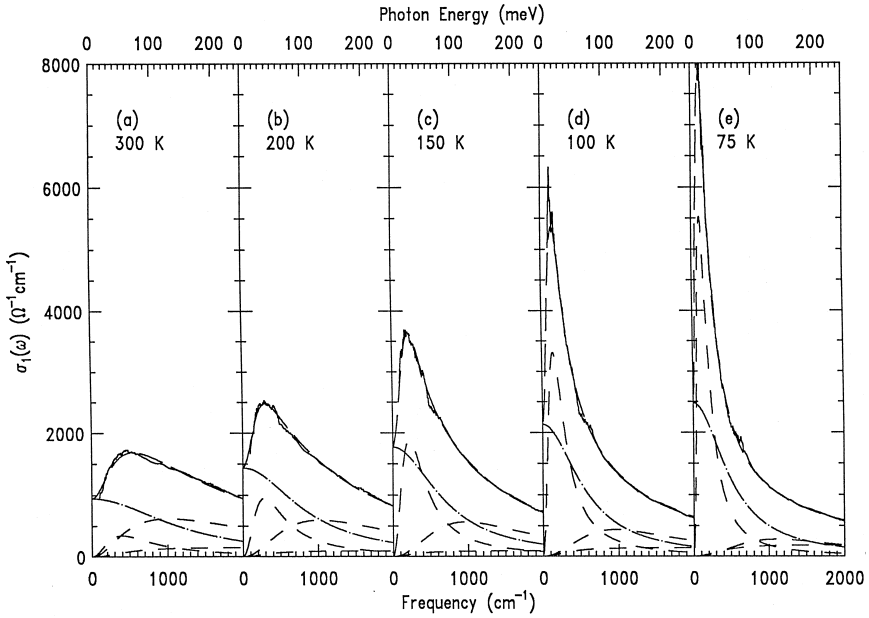

Fig. 5. The optical conductivity (solid line) of Ni-doped $Bi_2Sr_2CaCu_2O_{8+\delta}$ at 300, 200, 150, 100, and 75 K compared to conductivity (long dashed line) from the two-component oscillator fit. The various terms in the fits are also shown: the Drude band (dash–dotted line) and three Lorentz oscillators (short dashed line).

tral weight while its center frequency of the peak decreases from 420 to 106 cm^{-1}. One point that may be relevant for this mode is the likely presence of significant disorder induced by Ni impurities. The behavior may thus reflect the localization of carriers in the CuO_2 planes induced by Ni substitution. Indeed, a peak in the conductivity centered at finite frequency is a generic feature of disordered conductors and has been observed in disordered doped semiconductors [23–25] as well as conducting polymers [26]. Note that the Drude-like response persists with constant spectral weight while the peak at finite frequency produces the additional feature on the top of the Drude background. The Drude plasma frequency, $\omega_{pD} = 8500 \pm 200$ cm^{-1}, is essentially temperature-independent. The spectral weight of the additional peak grows with decreasing temperature, but never exceeds that of the Drude contributions.

In Fig. 6, we compare the temperature-dependent scattering rate $1/\tau_D$ for pure and Ni-doped crystals. It is clear from the plot that $1/\tau_D$ for both samples has a linear temperature dependence above T_c. However, the Ni-doped material has a larger scattering rate. Writing $\hbar/\tau_D = 2\pi\lambda_D k_B T + \hbar/\tau_0$ [27], where λ_D is the dimensionless coupling constant that couples the charge carriers to the temperature-dependent excitations responsible for the scattering and the temperature-independent term $1/\tau_0$ is assumed to result from elastic scattering by impurities. We obtain $\lambda_D \sim 0.28$ and $1/\tau_0 \sim 10$ cm^{-1} for pure Bi-2212 sample, $\lambda_D \sim 0.46$ and $1/\tau_0 \sim 282$ cm^{-1} for the Ni-doped sample. This result indicates that the effect of Ni on the conduction carriers is both to increase their elastic scattering rate and the coupling between the carriers and the excitation or the excitation itself. Using the Drude plasma frequency $\omega_{pD} \sim 8500$ cm^{-1} and the temperature dependence of $1/\tau_D$, the DC resistivity may be calculated [$\rho_{ir} = (\omega_{pD}^2 \tau_D/60)^{-1}$, in unit Ω cm]. This quantity is shown in the inset of Fig. 6, compared to transport measurements of a similar sample [9]. The DC resistivity deduced from the optical measurements is in fair agreement with the transport results, in particular with regard to the linear behavior in resistivity with decreasing temperature. However, the DC and far-infrared resistivity differ by about a factor of 2; at

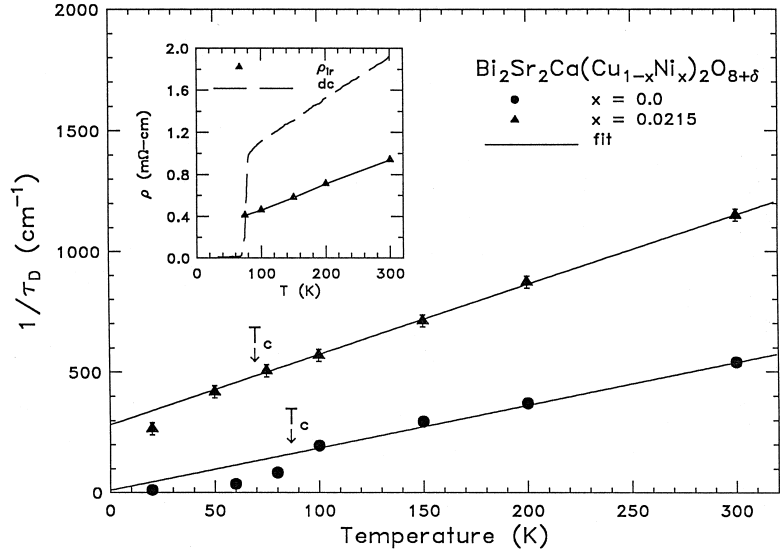

Fig. 6. The free carrier scattering rate $1/\tau_D$ (symbols) of the pure (filled circles) and Ni-doped (filled triangles) Bi-2212 crystals from the two-component fit (Eq. (2)). The straight line shows a linear fit to the temperature dependence of $1/\tau_D$ above T_c. The inset shows the infrared resistivity (filled triangles) from the optical measurements of Ni-doped $Bi_2Sr_2CaCu_2O_{8+\delta}$ and the DC resistivity from transport measurements (dashed line) of a similar sample [9].

300 K, $\rho_{DC} \sim 2\ m\Omega$ whereas $\rho_{ir} \sim 1\ m\Omega$. Additionally, there exists difference in the residual resistivity with a smaller nonzero intercept for our sample in a linear extrapolation to $T = 0$. The most possible origin for these discrepancies, as pointed out in Ref. [9], is that due to the irregular shape of the crystals after cleavage the absolute values of the DC resistivity are only approximate.

Below T_c, the quasiparticle scattering rate decreases quickly in pure Bi-2212, falling from the large values caused by inelastic scattering rate above T_c to a low value that is controlled by impurity scattering in the superconducting state. However, the addition of Ni so limits the decrease in $1/\tau_D$ that there is no indication of a drop in the scattering rate near T_c. Previous infrared measurements on Ni-doped Y123 films [21] have also found the fitted scattering rate decreases smoothly as T is lowered; no evidence for an abrupt change occurs near T_c. It is worth pointing out that the low temperature value of $1/\tau_D$ (20 K) approaches to zero in the pure sample. On the contrary, in the Ni-doped system, the $1/\tau_D$ is very close to the extrapolated intercept $1/\tau_0$ of the linear regime above T_c. This behavior must be taken into account in the later discussion of any property in the superconducting state that is sensitive to the impurity effects.

4.4. One-component analysis

It is instructive to explore the effects of Ni impurities on the frequency-dependent scattering rate within the so-called one component analysis of $\sigma_1(\omega)$. We first consider the generalized Drude analysis, in which the dielectric function is written as

$$\epsilon(\omega) = \epsilon_\infty - \frac{\omega_p^2}{\omega[m^*(\omega)/m][\omega + i/\tau^*(\omega)]}. \tag{3}$$

Here, $m^*(\omega)$ and $1/\tau^*(\omega)$ are the frequency-dependent (renormalized) mass and scattering rate of the charge carriers, and ω_p (the bare plasma frequency) $= \sqrt{4\pi ne^2/m^*}$, with n being the carrier density. Another quantity $1/\tau(\omega) = (m^*/m)1/\tau^*(\omega)$ represents the unrenormalized quasiparticle scattering rate. In the Ni-doped sample, the bare plasma frequency $\omega_p = 15\,650\ cm^{-1}$ can be determined from integrating optical conductivity up to the CT band in the sum-rule analysis.

Fig. 7 shows the frequency-dependent scattering rate $1/\tau(\omega)$ at several temperatures. Ni doping causes drastic changes in the room-temperature $1/\tau(\omega)$ as compared to the pure Bi-2212 sample, also shown in the inset of Fig. 7. For $x = 0.0$, the $1/\tau(\omega)$ increases with frequency in a linear fashion, as has been pointed out many times previously [28–30]. With Ni substitution, the scattering rate is enhanced over the entire spectral range. The frequency dependence is quite modest, and a $1/\omega$ behavior occurs at low frequency. The larger $1/\tau(\omega)$ for the Ni-doped crystal suggests an increase in elastic scattering. The $1/\omega$ behavior in the low-frequency $1/\tau(\omega)$ spectrum can be considered as related to localization of carriers in the CuO_2 planes initiated by Ni impurities. A similar behavior is also observed in disordered Tl2201 [19]. When the temperature is decreased from 300 to 75 K, $1/\tau(\omega)$ shifts significantly downward; changes with temperature below 75 K are much less prominent. The behavior of $1/\tau(\omega)$ differs from those of underdoped cuprates in two ways [31]. First, in underdoped materials the high-frequency part of $1/\tau(\omega)$ is effectively temperature-independent. Second, there is no indication of any suppression of $1/\tau(\omega)$ below a characteristic energy (the pseudogap state) for $T > T_c$.

A very similar approach was an expression for the dielectric function based on the marginal Fermi liquid (MFL) theory [32,33] and the nested Fermi liquid (NFL) theory [34,35]. The dielectric function can be written as

$$\epsilon(\omega) = \epsilon_\infty - \frac{\omega_p^2}{\omega[\omega - 2\Sigma(\omega/2)]}, \tag{4}$$

where the factors of 2 arise because quasiparticle excitations come in pairs. The quantity Σ is the quasiparticle self-energy of the charge carriers; and the imaginary part of Σ (essentially the scattering rate) is given by

$$-\mathrm{Im}\,\Sigma(\omega) \sim \begin{cases} \pi^2\lambda_T T, & \omega < T \\ \pi\lambda_\omega \omega, & \omega > T. \end{cases} \tag{5}$$

Here, λ_T or λ_ω is a dimensionless coupling constant. For $\omega < T$ the model predicts a renormalized scattering rate that is linear in temperature, which is expected from the linear temperature dependence in the resistivity that is observed in nearly all copper-oxide superconductors. As ω increases, reaching a magnitude of order of T or higher, quasiparticle interactions cause the scattering rate to grow linearly with

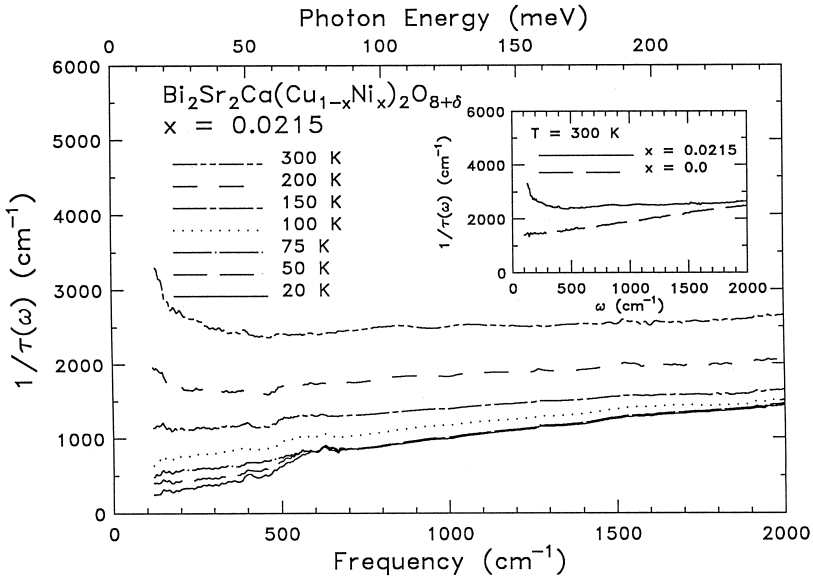

Fig. 7. The temperature-dependent quasiparticle scattering rate $1/\tau(\omega)$ obtained from the generalized Drude model (Eq. (3)) for Ni-doped $Bi_2Sr_2CaCu_2O_{8+\delta}$. The inset displays the room-temperature $1/\tau(\omega)$ spectra of the pure (dashed line) and Ni-doped (solid line) Bi-2212 crystals.

frequency up to a cutoff frequency ω_c that is introduced in the model.

$-\mathrm{Im}\,\Sigma(\omega)$ for the Ni-doped crystal is shown in Fig. 8. Clearly, Ni impurities induce a novel feature in the $-\mathrm{Im}\,\Sigma(\omega)$ spectra which is a region of the negative slope below ~ 250 cm^{-1}. This behavior of the scattering rate suggests that substitution with Ni strongly suppresses carrier mobility at low frequencies. A negative slope has been theoretically predicted for disordered two-dimensional conductor [36]. Above 250 cm^{-1}, the linear behavior of the scattering rate exists only up to ~ 1200 cm^{-1} at each temperature. This low cutoff frequency has been previously pointed out by Romero et al. [37] to imply that the MFL approach is limited to a narrow frequency range. It seems necessary to allow for a second component in the optical conductivity at higher frequencies. According to the MFL prescription, we calculate the slope of $-\mathrm{Im}\,\Sigma(\omega)$ between 250 and 1200 cm^{-1} at 300 K, which yields a coupling constant $\lambda_\omega \sim 0.06$. While at 75 K, this number is a factor of 2.5 larger, $\lambda_\omega \sim 0.15$. These results are much smaller than the coupling constant obtained from the Drude contribution only, $\lambda_D \sim 0.46$ (and much smaller than the 0.30 typically found in pure crystals [30]). This discrepancy suggests that one-component model of charge transport for the Ni-doped system where, $\sigma_1(\omega)$ shows a finite frequency peak in the far-infrared region rather than a smooth free-carrier band with excess conductivity at high frequencies, may be inappropriate.

4.5. Spectral weight

We now turn our attention to the temperature-dependent behavior of spectral weight shown in Fig. 9. The curves were obtained by using Eq. (1). There is some variation in normal-state $N_{\mathrm{eff}}(\omega)$ with temperature. As the temperature is reduced, the spectral weight first shifts to lower, but nonzero frequency; this is reflected in the progressive increase in the intensity of low-frequency conductivity with decreasing temperature shown in Fig. 3. In the superconducting state, $N_{\mathrm{eff}}(\omega)$ is smaller overall. The missing area in $\sigma_1(\omega)$ for the superconducting state appears in a δ function at $\omega = 0$, which is not included in the numerical integration of Eq. (1). The difference in $N_{\mathrm{eff}}(\omega)$ in the normal and superconducting states above and below T_c provides a good measure for the spectral weight in the superconducting condensate. We estimate the number of effective carriers per

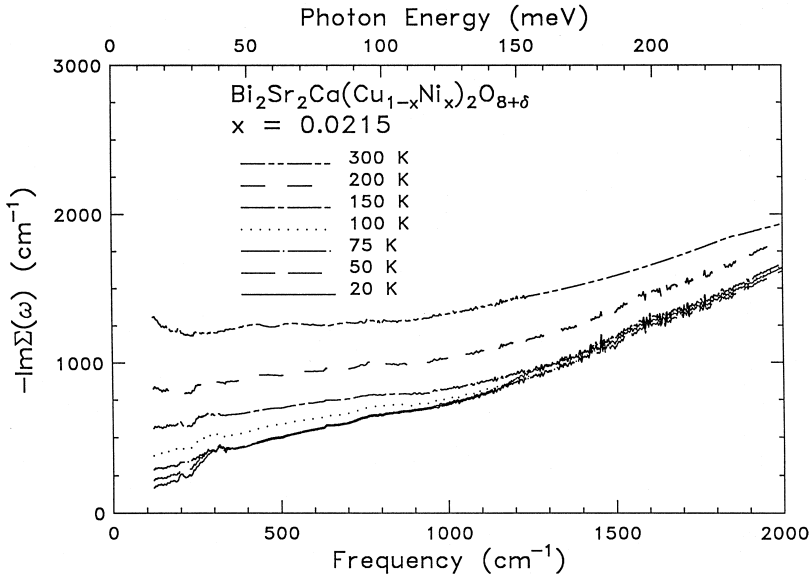

Fig. 8. The imaginary part of the self-energy $-\mathrm{Im}\,\Sigma(\omega)$ for Ni-doped $Bi_2Sr_2CaCu_2O_{8+\delta}$ obtained from the MFL theory (Eq. (4)) at several temperatures.

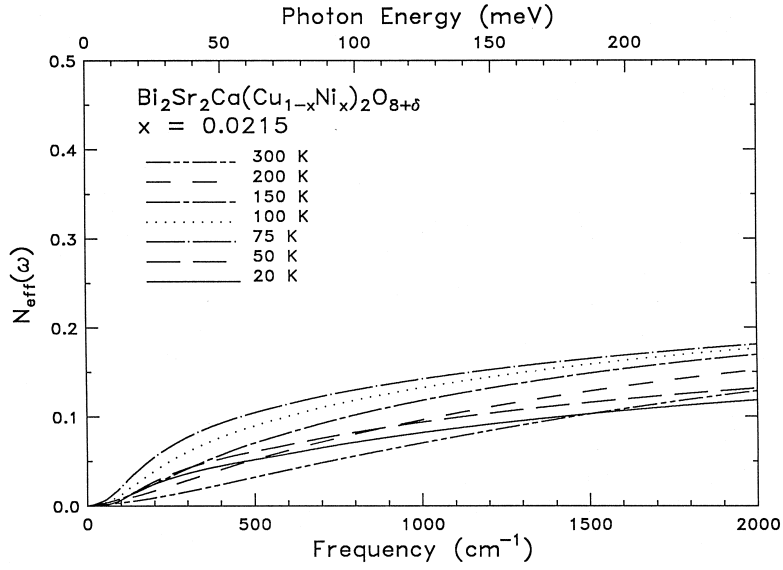

Fig. 9. The effective number of carriers per planar Cu atom as a function of frequency and temperature for Ni-doped $Bi_2Sr_2CaCu_2O_{8+\delta}$ obtained from an integration of the conductivity using Eq. (1).

copper in the superfluid $N_s = N_{eff}(75\ K) - N_{eff}(20\ K) = 0.062 \pm 0.01$. The value of the Drude plasma frequency from the two-component analysis is converted into the effective number of the free-carrier part, $N_{Drude} = 0.092 \pm 0.01$ per copper. The effective number of the total carriers is $N_{tot} = 0.34 \pm 0.03$. It turns out from the sum-rule analysis described above that the a fraction of N_s/N_{tot} and N_s/N_{Drude} is found to be 20 and 67%. Thus, only about a fifth of the total doping-induced spectral weight appears in the δ function at $\omega = 0$; the remainder is at finite frequencies. If the two-component picture is adopted, then 67% of the free-carrier spectral weight condenses, behavior that we discuss below.

4.6. Superconducting state properties

The inset of Fig. 3 compares the 20 K conductivity of pure and Ni-doped crystals. The 20 K $\sigma_1(\omega)$ remains finite in both crystals, down to the lowest frequencies. However, the pictures for $\sigma_1(\omega)$ in the Ni-doped material are quite different. Ni substitution does not produce a dirty-limit behavior as seen in conventional superconductors—an onset of absorption at 2Δ. Instead, the presence of Ni impurities yields low-frequency conductivity that is considerably larger than that of the pure Bi-2212. Moreover, the finite frequency peak that is centered around 400 cm^{-1} in the normal state moves below 100 cm^{-1} in the superconducting state. In view of this, we suggest that a peak centered at finite frequency is the result of impurity scattering rather than associated with the superconductivity. Nevertheless, a significant amount of residual conductivity in the Ni-doped crystal is consistent with the notion that only two thirds of the normal state spectral weight condenses into the superfluid at $T < T_c$. It is unlike clean-limit point of view [8,30] in the pure system, where nearly all of the Drude component collapses into the δ function.

In Fig. 10, we plot the superconducting transition temperature T_c as a function of n_s, where $n_s = N_s \cdot N_{Cu}/V_{cell}$ is the superfluid density, for a variety of pure and doped cuprates. The data points for the pure Y123 and Bi-2212 crystals lie on what is generally referred to as the Uemura line. This linear relationship between T_c and n_s has been observed in many underdoped and optimally-doped cuprates [41,42]. The data for the Ni-doped crystal are horizontally offset from the universal plot, with a smaller superfluid density than implied by T_c. The decreased superfluid density is most likely associated with impurity-induced disorder. Except for lightly Ni-doped (1.4%) Y123 single crystal [38], which lies

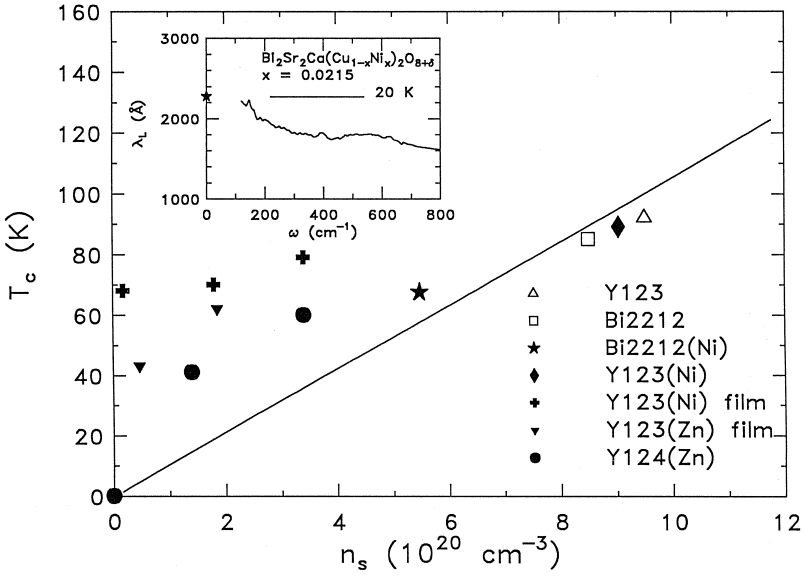

Fig. 10. T_c plotted a function of n_s in the CuO_2 planes determined by infrared spectroscopy for pure $YBa_2Cu_3O_{7-\delta}$ (open triangle) and $Bi_2Sr_2CaCu_2O_{8+\delta}$ (open square) single crystal [8], Ni-doped $Bi_2Sr_2CaCu_2O_{8+\delta}$ single crystal (filled star, this work), Ni-doped $YBa_2Cu_3O_{7-\delta}$ single crystal (filled diamond) [38], Ni-doped $YBa_2Cu_3O_{7-\delta}$ films (cross) [21,39,40], Zn-doped $YBa_2Cu_3O_{7-\delta}$ films (filled triangles) [21,40], and Zn-doped $YBa_2Cu_4O_8$ single crystals (filled circles) [22]. The solid curve is the so-called Uemura line [41,42]. (Inset) The frequency-dependent superconducting penetration depth $\lambda_L(\omega)$ of Ni-doped $Bi_2Sr_2CaCu_2O_{8+\delta}$ at 20 K. The values of $\lambda_L(0)$ from the sum-rule analysis are indicated by the symbol.

near the Uemura line, our results are like but smaller than the previous observations of very large reductions in superfluid density for Ni-doped (2, 4 and 6%) Y123 films [21,39,40]. In films, infrared measurements find no difference at all in $\sigma_1(\omega)$ between the normal and superconducting states. We also compare our Ni-doped results to Zn-doped data. As seen in Fig. 10, Zn-doped (2 and 4%) Y123 films [21,40] and Zn-doped (0.7, 1.4 and 3.5%) Y124 single crystals [22] reveal strong deviation from the Uemura line. This implies Ni impurities disturb the superconductivity much less than Zn impurities do. It has been discussed that the different levels of impurity concentration required to suppress superconductivity was attributed to magnetic pair breaking [43] and a decrease in the pairing potential [44] for Zn substitution and to weak magnetic pair-breaking for Ni substitution [44,45].

The strength of the superconducting condensate is related to the superconducting penetration depth $\lambda_L(\omega)$, defined as $\lambda_L(\omega) = \sqrt{c^2/4\pi\omega\sigma_2(\omega)}$ where c is the light speed and $\sigma_2(\omega)$ the imaginary part of the optical conductivity. The inset of Fig. 10 shows the frequency-dependent penetration depth $\lambda_L(\omega)$ of the Ni-doped crystal at 20 K. The fact that $\lambda_L(\omega)$ has an upturn trend below 300 cm^{-1} is an indication that not all of the free carriers have condensed into the δ function. The extrapolated zero-frequency value is about 2270 Å, which is much larger than the 1860 Å estimated for the pure Bi-2212 [8]. Note that a larger λ_L would correspond to a smaller superfluid density. The penetration depth may be used to calculate the plasma frequency of the condensate, $\lambda_L = c/\omega_{pS}$, a $\lambda_L(\omega \to 0) = 2270$ cm^{-1} yields $\omega_{pS} = 7010 \pm 200$ cm^{-1}. All of the above methods give consistent results for the spectral weight of the δ function.

5. Summary

In summary, we report the *ab*-plane optical reflectance of single crystal of $Bi_2Sr_2Ca(Cu_{1-x}Ni_x)_2O_{8+\delta}$, for $x = 0.0215$, over a wide frequency range above and below T_c. It is found that Ni doping

affects not only the normal state, but also the superconductivity. In the normal state, Ni substitution causes a drastic change in the frequency-dependent optical conductivity. Instead of $\sigma_1(\omega)$ monotonically decreasing with frequency at low frequencies (i.e., Drude behavior), a broad peak appears, centered at ~ 400 cm^{-1}, which grows in intensity and shifts to lower frequency as the temperature is reduced. A Drude-like contribution remains as well. The superconducting state conductivity is also anomalous. There is no sign of an energy gap, but a finite frequency peak in the normal state is still visible down to 20 K. It is important to realize that the observed bump in $\sigma_1(\omega)$ cannot be explained by the low-frequency extrapolation. We suggest that this peculiar low-frequency feature is associated with the significant disorder induced by Ni impurities.

Based on the conductivity data, we have investigated the behavior of the quasiparticle scattering rate through Ni substitution within both two-component and one-component pictures. The normal-state $1/\tau_D$ of the Drude contribution shows that the primary effect of Ni on the conduction carriers is to increase their elastic scattering rate. There is no indication of a rapid drop in $1/\tau_D$ just below T_c as compared to the pure Bi-2212. Alternatively, the frequency-dependent scattering rate obtained from the generalized Drude model and MFL theory suggests that Ni also acts as an impurity and the effect is additive. A $1/\omega$ behavior in the low-frequency scattering rate spectra can be considered as localization of carriers in the CuO_2 planes initiated by Ni impurities.

Estimate of the low-frequency spectral weight shows that Ni reduces the carrier density in the CuO_2 plane: each Ni removes one carrier. Below T_c, we observe a decrease of low-frequency spectral weight in the conductivity spectra, although there is a lot of low-energy oscillator strength remaining. The superconducting penetration depth, calculated from this missing area, is about 2270 Å. A sum-rule evaluation finds the superfluid contains about a fifth of the total doping-induced, or two thirds of the free-carrier oscillator strength in the normal state. The strength of the condensate is horizontally offset from the Uemura line, with a smaller superfluid density than implied by T_c. This decreased superfluid density in the CuO_2 plane could be connected with the effect of impurity-induced disorder.

We can compare the optical data with other experimental results, including ARUPS and microwave measurements. Room-temperature ARUPS spectra [9] for a crystal similar to ours show that Ni doping affects the electronic band structure. The disappearance of the dispersing band-like state suggests a modification of the Fermi surface. There is an evidence for the spectral weight shifting from the dispersing band-like state into an incoherent background of states elastically scattered by Ni impurities. In agreement with our results, Ni acts primarily to induce disorder and leads to a radical alteration of the Drude feature into finite frequency peak in the conductivity spectra. There is a connection between the impurity studies presented here and the microwave results [46]. We note a resemblance of the scattering rate $1/\tau_D$ from the free-carrier contributions to the microwave data obtained with the Ni-doped Y123 single crystals. Surface impedance results indicate that Ni impurities provide strong elastic scattering that limits the collapse of the scattering rate near T_c and suppresses the peak in the surface resistance. Furthermore, comparison of the effect of Ni and Zn impurities on the temperature dependence of the London penetration depth suggests that Ni does not have such a strong pair-breaking effect as Zn impurity, which is also consistent with our observations on the behavior of the superfluid density.

Acknowledgements

We thank Steve Thomas for the AC susceptibility measurements. This work at the University of Florida is supported by the National Science Foundation, Grant No. DMR-9403894.

References

[1] J.T. Markert, Y. Dalichaouch, M.B. Maple, in: D.M. Ginsberg (Ed.), Physical Properties of High Temperature Superconductors, World Scientific, Singapore, 1989, p. 265.
[2] A.A. Abrikosov, L.P. Gor'kov, Zh. Eksp. Teor. Fiz. 35 (1950) 1558.
[3] A.A. Abrikosov, L.P. Gor'kov, Sov. Phys. JETP 8 (1959) 1090.
[4] P.W. Anderson, J. Phys. Chem. Solids 11 (1959) 26.

[5] D.B. Romero, C.D. Porter, D.B. Tanner, L. Forró, D. Mandrus, L. Mihaly, G.L. Carr, G.P. Williams, Phys. Rev. Lett. 68 (1992) 1590.
[6] M.A. Quijada, D.B. Tanner, R.J. Kelley, M. Onellion, Z. Phys. B 94 (1994) 255.
[7] M.A. Quijada, PhD Thesis, Department of Physics, University of Florida, 1994.
[8] H.L. Liu, M.A. Quijada, A. Zibold, Y.-D. Yoon, D.B. Tanner, G. Cao, J.E. Crow, H. Berger, G. Margaritondo, L. Forró, O. Beom-Hoan, J.T. Markert, R.J. Kelly, M. Onellion, J. Phys.: Condens. Matter 11 (1999) 239.
[9] C. Quitmann, P. Almeras, J. Ma, R.J. Kelley, H. Berger, C. Xueyu, G. Margaritondo, M. Onellion, Phys. Rev. B 53 (1996) 6819.
[10] I. Terasaki, S. Tajima, H. Eisaki, H. Takagi, K. Uchinokura, S. Uchida, Phys. Rev. B 41 (1990) 865.
[11] F. Wooten, Optical Properties of Solids, Academic Press, New York, 1972.
[12] H. Eisaki, S. Uchida, J. Phys. Chem. Solids 56 (1995) 1811.
[13] M.K. Kelly, P. Barboux, J.-M. Tarascon, D.E. Aspnes, Phys. Rev. B 40 (1989) 6797.
[14] Y.-Y. Wang, A.L. Ritter, Phys. Rev. B 43 (1991) 1241.
[15] D.M. Ori, A. Goldoni, U. del Pennino, F. Parmigiani, Phys. Rev. B 52 (1995) 3727.
[16] M. Reedyk, T. Timusk, Phys. Rev. B 69 (1992) 2705.
[17] A.A. Tesvetkov, J. Schützmann, J.I. Gorina, G.A. Kaljushnaia, D. van der Marel, Phys. Rev. B 55 (1997) 14152.
[18] M. Reedyk, PhD Thesis, McMaster University, 1992.
[19] A.V. Puchkov, T. Timusk, S. Doyle, A.M. Hermann, Phys. Rev. B 51 (1995) 3312.
[20] D.N. Basov, A.V.R.A. Hughes, T. Strach, J. Preston, T. Timusk, D.A. Bonn, R. Liang, W.N. Hardy, Phys. Rev. B 49 (1994) 12165.
[21] J.-T. Kim, T.R. Lemberger, S.R. Foltyn, X. Wu, Phys. Rev. B 49 (1994) 15790.
[22] D.N. Bosov, B. Dabrowski, T. Timusk, Phys. Rev. Lett. 81 (1998) 2132.
[23] A. Gold, S.J. Allen, B.A. Wilson, D.C. Tsui, Phys. Rev. B 25 (1982) 3519.
[24] H.K. Ng, M. Capizzi, G.A. Thomas, R.N. Bhatt, A.C. Gossard, Phys. Rev. B 33 (1986) 7329.
[25] H.F. Jang, G. Cripps, T. Timusk, Phys. Rev. B 41 (1990) 5152.
[26] K. Lee, R. Menon, C.O. Yoon, A.J. Heeger, Phys. Rev. B 52 (1995) 4779.
[27] P.B. Allen, T.P. Beaulac, F.S. Khan, W.H. Butler, F.J. Pinski, J.C. Swihart, Phys. Rev. B 34 (1986) 4331.
[28] T. Timusk, D.B. Tanner, in: D.M. Ginsberg (Ed.), Physical Properties of High Temperature Superconductors Vol. I, World Scientific, Singapore, 1989, pp. 339.
[29] G.A. Thomas, in: D.P. Tunstall, W. Barford, (Eds.), Proceeding of the Thirty-Ninth Scottish Universities Summer School in Physics of High Temperature Superconductivity, Adam Hilger, Bristol, 1991, p. 169.
[30] D.B. Tanner, T. Timusk, in: D.M. Ginsberg, (Ed.), Physical Properties of High Temperature Superconductors III, World Scientific Press, 1992, p. 363.
[31] A. Puchkov, D.N. Bosov, T. Timusk, J. Phys. Condens. Matter 8 (1996) 10049.
[32] C.M. Varma, P.B. Littlewood, S. Schmitt-rink, E. Abrahams, A.E. Ruckenstein, Phys. Rev. Lett. 63 (1989) 1996.
[33] P.B. Littlewood, C.M. Varma, J. Appl. Phys. 69 (1991) 4979.
[34] A. Virosztek, J. Ruvalds, Phys. Rev. B 42 (1990) 4064.
[35] C.T. Rieck, W.A. Little, J. Ruvald, A. Virosztek, Phys. Rev. B 51 (1995) 3772.
[36] P.B. Allen, Phys. Rev. B 3 (1971) 305.
[37] D.B. Romero, C.D. Porter, D.B. Tanner, L. Forró, D. Mandrus, L. Mihaly, G.L. Carr, G.P. Williams, Solid State Commun. 82 (1992) 183.
[38] C.C. Homes, Q. Song, B.P. Clayman, D.A. Bonn, R. Liang, W.N. Hardy, SPIE Proc. 2696 (1996) 82.
[39] M.J. Sumner, J.-T. Kim, T.R. Lemberger, Phys. Rev. B 47 (1993) 12248.
[40] E.R. Ulm, J.-T. Kim, T.R. Lemberger, S.R. Foltyn, X. Wu, Phys. Rev. B 51 (1995) 9193.
[41] Y.J. Uemura, G.M. Luke, B.J. Sternlieb, J.H. Brewer, J.F. Carolan, W.N. Hardy, R. Kadono, J.R. Kempton, R.F. Kiefl, S.R. Kreitzman, P. Mulhern, T.M. Riseman, D.Ll. Williams, B.X. Yang, S. Uchida, H. Takagi, J. Gopalakrishnan, A.W. Sleight, M.A. Subramanian, C.L. Chien, M.Z. Cieplak, G. Xiao, V.Y. Lee, B.W. Statt, C.E. Stronach, W.J. Kossler, X.H. Yu, Phys. Rev. Lett. 62 (1989) 2317.
[42] Y.J. Uemura, L.P. Le, G.M. Luke, B.J. Sternlieb, W.D. Wu, J.H. Brewer, T.M. Riseman, C.L. Seaman, M.B. Maple, M. Ishikawa, D.G. Hinks, J.D. Jorgensen, G. Saito, H. Yamochi, Phys. Rev. Lett. 66 (1991) 2665.
[43] A.V. Mahajan, H. Alloul, G. Collin, J.F. Marucco, Phys. Rev. Lett. 72 (1994) 3100.
[44] P. Monthoux, D. Pines, Phys. Rev. B 49 (1994) 4261.
[45] P. Mendels, H. Alloul, G. Collin, N. Blanchard, J.F. Marucco, J. Bobroff, Physica C 235–240 (1994) 1595.
[46] D.A. Bonn, S. Kamal, K. Zhang, R. Liang, D.J. Baar, E. Klein, W.N. Hardy, Phys. Rev. B 50 (1994) 4051.